CHAPTER FIFTEEN

Reconstitution of Contractile Actomyosin Arrays

Michael Murrell[*], **Todd Thoresen**[†,‡], **Margaret Gardel**[†,‡,1]

[*]Departments of Biomedical Engineering and Materials Science and Engineering, University of Wisconsin, Madison, Wisconsin, USA
[†]Department of Physics, Institute for Biophysical Dynamics, University of Chicago, Chicago, Illinois, USA
[‡]James Franck Institute, University of Chicago, Chicago, Illinois, USA
[1]Corresponding author: e-mail address: gardel@uchicago.edu

Contents

Abstract

Networks and bundles comprised of F-actin and myosin II generate contractile forces used to drive morphogenic processes in both muscle and nonmuscle cells. To elucidate the minimal requirements for contractility and the mechanisms underlying their contractility, model systems reconstituted from a known set of purified proteins *in vitro* are needed. Here, we describe two experimental protocols our lab has developed to reconstitute 1D bundles and quasi-2D networks of actomyosin that are amenable to quantitative biophysical measurement. These assays have enabled our discovery of the mechanisms of contractility in disordered actomyosin assemblies and of a mechanical feedback between contraction and F-actin severing.

Methods in Enzymology, Volume 540
ISSN 0076-6879
http://dx.doi.org/10.1016/B978-0-12-397924-7.00015-7

1. INTRODUCTION

The action of myosin II motors on the actin cytoskeleton generates contractile forces that are used in a myriad of morphogenic processes including cell division and migration, as well as the formation and maintenance of multicellular tissue. While the necessity of actomyosin for contractility in these processes is nearly universally conserved, its organization varies widely. In striated muscle, actomyosin is found in sarcomeres with highly regulated F-actin polarity and length. Contraction of sarcomeric actomyosin is well described by the sliding filament models of muscle contraction (Huxley, 2004). By contrast the actomyosin in smooth muscle and nonmuscle cells is typically arranged in bundles or network that lack sarcomeric organization and are "disorganized" with respect to F-actin polarity, lengths, and orientation. In such disordered arrangements, new physical models are needed to describe contractility.

As part of an effort to understand the physico-chemical origins of striated and smooth muscle contractility, reconstitutions of actin and myosin II have been studied for over 60 years. Solutions of actin and myosin were isolated from muscle tissue and supplemented with ATP which resulted in changes in its optical and mechanical properties (Dainty et al., 1944; Szent-Györgyi, 1945, 1947, 1950). These actomyosin solutions exhibited "superprecipitation", an increase in actomyosin density and viscosity, which implied F-actin network "contractility" (Spicer, 1951). Further studies outlined the requisite components of the contractile machinery by establishing stoichiometric relationships between actin, myosin, and actin-binding proteins (Ebashi & Ebashi, 1964; Janson, Kolega, & Taylor, 1991; Stossel, Hartwig, Yin, Zaner, & Stendahl, 1982; Watanabe & Yasui, 1965; Weber & Winicur, 1961). Thus, these early studies identified a minimal "parts list" for reconstructing contractile actomyosin assemblies.

Missing from these early studies was recapitulation of actomyosin organizations found in cells (e.g., bundles or 2D cortex rather than dilute 3D gels) and a mechanistic understanding of how contractility is regulated in diverse actomyosin organizations. Here, we describe methods for constructing actomyosin bundles and networks that are more faithful mimics to those found in living cells. These assays have enabled our studies of contractility, self-organization, and feedback in disordered actomyosin bundles and networks (Lenz, Thoresen, Gardel, & Dinner, 2012; Murrell & Gardel, 2012; Stachowiak et al., 2012; Thoresen, Lenz, & Gardel, 2011, 2013).

2. REAGENTS

2.1. Protein purification and filament formation

Myosin purification: All purification takes place at 4 °C. Native smooth muscle myosin is purified from fresh chicken gizzards essentially as described previously (Bárány, 1996), except myosin is actively phosphorylated using myosin light chain kinase prior to storage in order to minimize heterogeneity due to phosphorylation-dependent configuration. Nonmuscle myosin was purified similarly using expired human platelets obtained at a local blood bank. Skeletal muscle myosin was purified as described previously (Margossian & Lowey, 1982; Pollard, 1982) or purchased from Cytoskeleton, Inc. Fluorescent labeling of myosin is performed using a maleimide dye (Molecular Probes, Invitrogen) that readily reacts with available cysteine residues as described previously (Thoresen et al., 2011); the labeling methods are identical between skeletal, smooth, and nonmuscle isoforms with a typical labeling ratio of 3.6 dye per myosin dimer. Myosin is concentrated using Amicon Ultra-15 centrifugal filters (Millipore, 100 kDa cutoff) to a high concentration (~18 mg/mL) in Myosin Storage Buffer (5 m*M* Pipes, pH 7.0, and 0.45 *M* KCl), then flash frozen in liquid nitrogen for long-term storage at −80 °C.

Myosin thick filament formation: Flash-frozen aliquots of fluorescently labeled and phosphorylated myosin are rapidly thawed. To separate the fraction of myosin dimers that binds with high affinity to F-actin in saturating ATP (and presumed to be enzymatically dead) from the fraction that binds with weak affinity to F-actin in saturating ATP (and presumed to be enzymatically active), myosin dimers are mixed with phalloidin-stabilized F-actin at a 1:5 myosin:actin molar ratio in Spin-down Buffer (20 m*M* MOPS, pH 7.4, 500 m*M* KCl, 4 m*M* $MgCl_2$, 0.1 m*M* EGTA, 500 μ*M* ATP) and centrifuged for 30 min at 100,000 × *g*. The supernatant contains myosin with low affinity to F-actin, whereas the high-affinity binding fraction cosediments with the F-actin pellet. Myosin protein concentrations are determined spectroscopically using an extinction coefficient at 280 nm of 0.56 mL/mg/cm compared to a myosin-free sample that includes nucleotide.

For bundles described in Section 3, myosin thick filaments are formed by diluting myosin in Assay Buffer with varied KCl concentration to control thick filament size. By varying the KCl concentration from 100 to 200 m*M* KCl, the average lengths of skeletal muscle myosin thick filaments

changed from 1.5 to 0.5 μm and smooth muscle myosin filaments changed from 1.2 to 0.7 μm (Thoresen et al., 2013). Further modulation of myosin filament lengths is possible by altering the final salt conditions and/or the rate of salt dilution (Thoresen et al., 2013). For the cortex assay described in Section 4, myosin dimers are added directly to the actin cortex contained in F-buffer and myosin thick filaments polymerize *in situ*.

Actin purification: Actin is purified from rabbit skeletal muscle acetone powder and stored in G-buffer (pH 8.0, 2 m*M* Tris–HCl, 0.2 m*M* ATP, 0.2 m*M* $CaCl_2$ 0.2 m*M* DTT, 0.005% NaN_3) at −80 °C. Biotinylated actin is prepared using EZ-Link NHS-PEO_4 biotinylation kit (Thermo Scientific).

Actin filament preparation: To form biotinylated actin filaments, biotinylated G-actin is mixed with unlabeled G-actin in a 1:10 stoichiometry prior to polymerization. G-actin is polymerized by addition of F-buffer (10 m*M* imidazole, pH 7.0, 1 m*M* $MgCl_2$, 50 m*M* KCl, 2 m*M* EGTA, 0.5 m*M* ATP). Fluorescently labeled phalloidin is added in a 2:1 mole ratio (phalloidin:actin) to both stabilize F-actin and for visualization in fluorescence imaging.

2.2. Microscopy

Fluorescence imaging is performed using a Ti-E microscope body (Nikon) fitted with a CSU-X spinning disc confocal head (Yokogawa), a HQ2 CoolSnap CCD camera (Roper Scientific), and a 60 × 1.2NA water immersion objective lens (Nikon). The instrument is controlled with Metamorph software (MDS Analytical Technologies).

3. RECONSTITUTED ACTOMYOSIN BUNDLES

Actomyosin bundles are assembled and contracted within a flow cell through a particular sequential addition of components. The bundles formed by the following method contain ∼5 F-actin per cross-section and are 5–50 μm in contour length. Because bundles form without the enforcement of F-actin polarity, they are considered polarity disordered. The F-actin and myosin are both fluorescently labeled to facilitate direct observation by confocal microscopy during myosin II activity. The ends of bundles are tethered to avidin beads coupled to an elastic substrate to permit force measurement. Measurement of bundle contraction after a breakage event permits measurement of unloaded contraction velocity. The unloaded contraction rate and

tension generated are modulated by varying myosin II isoform, filament density, and quantity (Thoresen et al., 2011, 2013).

3.1. Reagents

3.1.1 Avidin beads

3 μm diameter polystyrene carboxylate beads (Polysciences) are biotinylated using EZ-Link NHS-PEO_4 biotinylation kit (Thermo Scientific) and subsequently incubated in 5 mg/mL neutravidin (Thermo Scientific) to coat the beads. The beads are repeatedly spun down (15,000 × *g*, 5 min) and resuspended 10 times in PBS to remove unbound neutravidin. The beads are then briefly sonicated and stored at 4 °C undergoing constant rotation.

3.1.2 Acrylamide gels

A polyacrylamide (PAA) gel is polymerized on the coverslip surfaces (22 mm diameter #1½, EMS). Predetermined acrylamide and bisacrylamide concentrations are used to form gels with a known shear elastic moduli which can be confirmed through measurement with a stress-controlled rheometer (Aratyn-Schaus, Oakes, Stricker, Winter, & Gardel, 2010). 1 mg/mL biotinylated bovine serum albumin (BSA), formed by reacting BSA (Sigma) with NHS-Biotin (Thermo Scientific) is covalently attached to the gel surface using sulfo-SANPAH (Thermo Scientific). Cover slips are washed in PBS, stored at 4 °C and used within 2 weeks.

3.1.3 Sample chamber

A flow chamber customized for imaging with high numerical aperture objectives and small (~30 μL) exchange volumes was designed and obtained from Chamlide (www.chamlide.com). A picture of the flow chamber is in Fig. 15.1A.

3.2. Actomyosin bundle construction

The sequential addition and incubation of sample components is used to template the assembly of bundles existing predominately within a single confocal imaging plane and tethered to surface-bound beads at their ends to facilitate force measurement. First, a 10–20-μm thick PAA gel is formed on a coverslip and biotinylated BSA is covalently attached to the top surface as described above. This biotinylated BSA-PAA substrate provides a surface largely inert to nonspecific myosin or actin binding and facilitates traction force microscopy. The substrate is then loaded into the custom flow

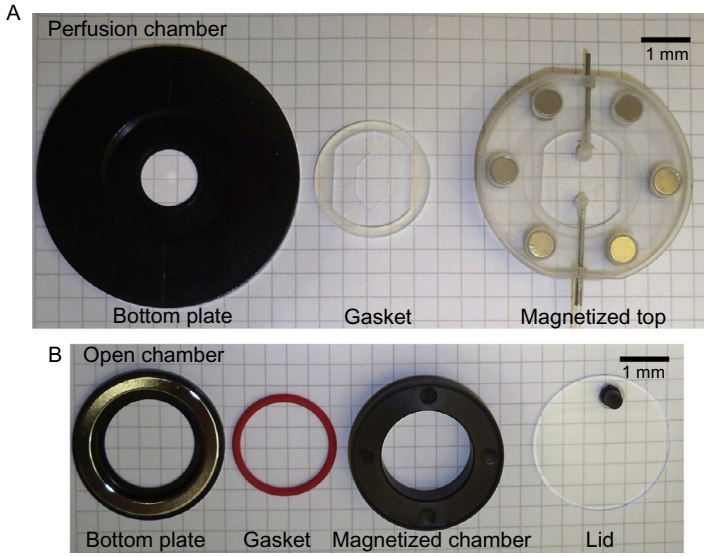

Figure 15.1 Photographs of custom sample chambers used in experiments. In (A), a perfusion chamber consists of a bottom anodized aluminum plate that holds a glass coverslip, a rubber gasket, and a magnetized top plate with molded inlet/outlet for fluid exchange. In (B), an open chamber comprised of an anodized aluminum bottom plate to hold coverslip with magnetized ring, a rubber gasket, magnetized chamber, and colorless top.

chamber. After assembling the perfusion chamber, water is perfused through the sample to maintain hydration of PAA gel prior to starting the experiment.

A dilute suspension of 3 μm diameter neutravidin beads in Wash Buffer (20 m*M* MOPS, pH 7.4, 50 m*M* KCl, 4 m*M* $MgCl_2$, 0.1 m*M* EGTA) is perfused into the perfusion chamber and incubated for ~10 min to allow for the beads to sediment and bind to the biotinylated-BSA surface (Fig. 15.2A, panel 1). Unbound beads are then removed by further perfusion of Wash Buffer. We aim for an average distance between beads >10 μm. Phalloidin-stabilized F-actin containing 10% biotinylated G-actin is gently sheared to a length of ~5–6 μm, diluted to 1 μ*M* in Assay Buffer (20 m*M* MOPS, pH 7.4, 100 m*M* KCl, 4 m*M* $MgCl_2$, 0.1 m*M* EGTA, 0.7% methylcellulose, 0.25 mg/mL glucose, 0.25% β-mercaptoethanol, 0.25 mg/mL glucose oxidase, 35 μg/mL catalase) and perfused into the chamber. Over the course of 30 min, F-actin binds to the neutravidin beads. A majority of free, unbound F-actin is removed by perfusion of two chamber volumes

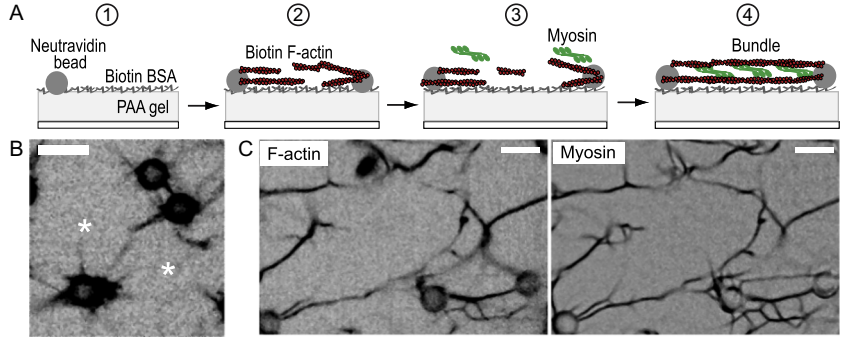

Figure 15.2 (A) Schematic illustrating the sequential process used for templated bundle assembly. (1) Biotinylated-bovine serum albumin is coupled to the surface of a PAA gel affixed to a glass coverslip. Neutravidin beads (gray circles) bind to the biotinylated-bovine serum albumin. (2) Biotinylated F-actin (red) is introduced and binds to beads. A dilute suspension of F-actin remains. (3) Myosin thick filaments (green) suspended in nucleotide-free Assay Buffer (black) are introduced. (4) F-actin cross-linking by myosin filaments mediates bundle formation. (B) Inverted contrast image of F-actin asters visualized with Alexa 568-phalloidin before myosin perfusion. Dark circles are F-actin-coated beads. Asterisks indicate free F-actin ends. Scale bar is 5 μm. (C) Inverted contrast images of F-actin visualized with Alexa 568-phalloidin (left) and OG-labeled myosin (right) illustrating network of bundles formed after 30 min incubation of F-actin asters with myosin thick filaments. Scale bar is 5 μm.

of Assay Buffer. The remaining bead-bound F-actin provides sites to template the assembly of actomyosin bundles (Fig. 15.2A, panel 2, B). Since biotinylated G-actin is randomly incorporated into F-actin during polymerization, free F-actin ends emanating from beads are likely of random polarity. The formation of F-actin asters is not sensitive to small changes in wash steps, but is extremely sensitive to air bubbles within the flow chamber.

Preformed myosin II thick filaments are then perfused in with Assay Buffer lacking ATP. A dialysis against Storage buffer supplemented with 0.2 m*M* EGTA is performed to ensure complete removal of nucleotide using "drop dialysis" technique with 2.5 nm VSWP membrane (Millipore) and gentle stirring for 2 h at 4 °C. It is crucial that all free nucleotide is removed to prevent motor catalysis during bundle formation. Myosin II filaments cross-link F-actin bound to beads to F-actin remaining in solution to form a quasi-2D network of bundles bound to the beads (Fig. 15.2A, panels 3 and 4, C, and D). Myosin motor activity is then initiated by the introduction of Assay Buffer containing 0.1–1 m*M* ATP.

3.3. Force measurement

Because the stiffness of the underlying PAA gel substrate is tunable, and its elastic properties are well known, forces from an individual contracting bundle can be directly measured by measuring the Hookian displacements of the streptavidin beads linking the bundle to the gel, concurrent with the observation of bundle dynamics. Using traction force reconstruction with point forces to calculate force from a displacement field on the top surface of a PAA gel, the force is related to the local gel displacement by an effective spring constant, k_{eff}. As expected, k_{eff} varies linearly with the PAA gel stiffness (Thoresen et al., 2011) (Fig. 15.3). Assuming deformation of the polystyrene bead ($G' \sim 10^9$ Pa) is negligible compared to that of the soft PAA gel ($G' = 54$–600 Pa), the bead displacement is then multiplied by the k_{eff} to measure the force produced during contraction. A significant caveat to this approach is that this does not consider effects of poor bead attachment to the substrate and/or its rotation within the soft gel. Improvements to the forces measurements are ongoing.

4. BIOMIMETIC CORTEX

The reconstituted actomyosin cell cortex is created adjacent to a standard glass coverslip, in a layer-by-layer assembly of lipids and proteins (Fig. 15.4). The order of assembly is as follows: (1) formation of a bilayer membrane on the coverslip, (2) the addition of membrane-F-actin attachment factors that bind the membrane, (3) the addition of F-actin that couples to the surface of the membrane, (4) the addition of F-actin cross-linking proteins, and finally, (5) the addition of myosin II dimers that assemble into filaments *in situ*. The resultant network is highly disordered and quasi-2D. The membrane, F-actin, and myosin II are fluorescently labeled, and thus can be observed during contraction. The extent of network contraction is modulated by changing the extent of F-actin membrane coupling, cross-linking, and concentration of myosin II motors (Murrell & Gardel, 2012).

4.1. Reagents

4.1.1 Sample chamber

An open chamber with ~500 μL sample volume amenable to high numerical optics was designed and obtained from Chamlide (www.chamlide.com); a picture of the chamber is shown in Fig. 15.1B. After cortex assembly, the chamber is covered with a coverslip to prevent evaporation of contents.

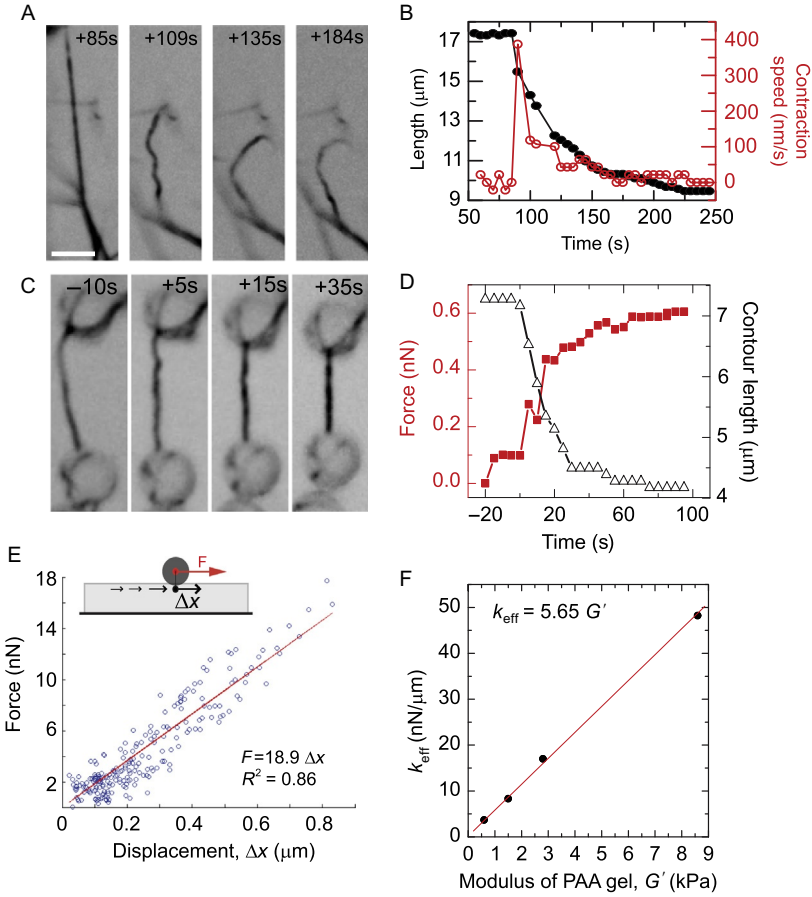

Figure 15.3 Contraction of tethered and untethered bundles. (A) Time-lapse series of inverted contrast, OG-myosin images in a contracting bundle with $R_{M:A} = 1.4$. Times are in seconds before (negative times) or after (positive times) addition of 0.1 m*M* ATP. A connection to a neighboring bundle breaks between 60 and 65 s (arrow), following which contraction of both the untethered bundle (asterisk) and tethered bundle (dashed line) resume. Scale bar is 5 μm. (B) Contour length (left axis, solid circles) and contraction speed (right axis, open circles) of the bundle indicated by the dashed line in (A). (C) Time-lapse series of inverted contrast OG-myosin images illustrating the contraction of a bundle tethered to beads at both ends. Bundle shown contains $R_{M:A} = 1.4$. Scale bar, 5 μm. (D) Bundle contour length (open triangles, right axis) and force (left axis, closed squares) versus time for bundle contraction shown in (C). (E) The calibration of force (in nN) as a function of bead displacement (in mm) to obtain the effective spring constant k_{eff} for a PAA gel with $G' = 2.8$ kPa obtained from Traction Force Reconstruction from Point Forces. (F) The effective spring constant as a function of G'.

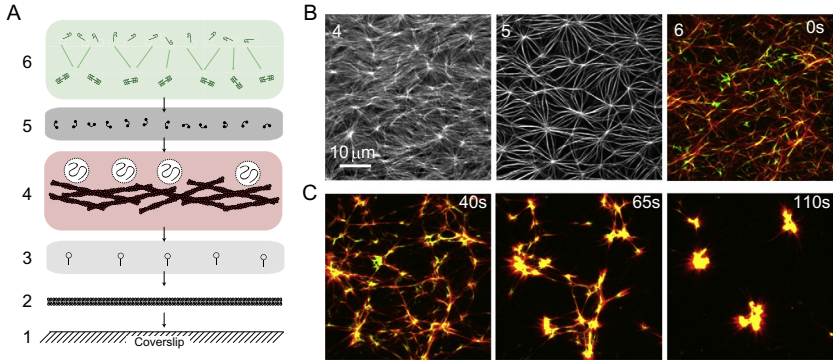

Figure 15.4 Assembly of a contractile model cortex. (A) Schematic of stepwise cortex assembly: (1) Piranha-treated coverslip, (2) phospholipid bilayer formed on coverslip, (3) incubation with F-actin-membrane attachment factors, (4) crowding of F-actin (F-actin in red, methylcellulose in circles), (5) F-actin cross-linking, and (6) myosin II addition. (B) Fluorescence images of (left) F-actin without cross-linker (Stage 4), (middle) with 30 n*M* α-actinin (Stage 5), and (right) 40 n*M* skeletal muscle myosin II (Stage 6). (C) Time course of contraction, 40, 65, and 110 s after the addition of myosin thick filaments. Red is actin, green is myosin.

4.1.2 Coverslips

Coverslips are hydroxylated with a 1:3 mixture of 30% hydrogen peroxide (Sigma) and sulfuric acid (Piranha Etching) to make them sufficiently hydrophilic for membrane attachment. Slowly, the peroxide is added to the acid within a Pyrex container containing 25-mm coverslips, which is stirred slowly for 15 min. The coverslips are then washed repeatedly in water, and then stored in methanol. Due to the quick decomposition of the hydrogen peroxide, Piranha solution must be freshly prepared and never stored. Proper safety precautions should be taken as Piranha solutions are volatile and generate large amounts of heat and gas (e.g., http://web.mit.edu/cortiz/www/PiranhaSafety.doc). Consult your local lab safety officials.

4.1.3 Construction of lipid bilayer

The bilayer is formed on the hydroxylated coverslips in the following series of steps:

1. Add 2.5 mg lipids (in combinations listed in Table 15.1) dissolved in chloroform to a glass vial, and then dry them under N_2 gas for 5 min.
2. Add 5 mL Vesicle Buffer (100 m*M* NaCl, 0.1 m*M* EDTA, pH 7.3) to the glass vial and cover with parafilm or a nonscrew plastic top. Vortex

Table 15.1 Compositions of the lipid bilayer membrane

Lipid	For attachment	No attachment
Egg phosphatidyl choline (EPC)	91%	99.8%
1,2-Di-(9Zoctadecenoyl)-*sn*-glycero-3-([*N*-(5-amino-1-carboxypentyl)iminodiacetic acid]succinyl) (NTA-Ni)	8.8%	0
Oregon Green 1,2-dihexadecanoyl-*sn*-glycero-3-phosphoethanolamine (OG-DHPE)	0.2%	0.2%

the lipid solution for 10 s to resuspend the lipids. After vortexing, the vesicle solution is cloudy, reflecting the formation of multilamellar vesicles which scatter light.

3. Sonicate the vesicle solution in a bath sonicator until the solution becomes clear. Use either a ring stand and test tube clamp, or other methods for suspending the glass vial a few millimeters into the water bath. When sonication is complete, the vesicle solution is clear because multilamellar vesicles are broken into small, unilamellar vesicles (SUVs) which are approximately 50–100 nm in diameter. The vesicle solution can be kept at 4 °C for up to 1 week, although is sonicated prior to reuse.
4. The clear SUV solution is then added to the Chamlide chamber sandwiching the Piranha-treated coverslip, which is immersed in 0.5–1 mL of Vesicle Buffer. The SUV solution is allowed to incubate in the chamber for 15 min in the dark to prevent bleaching of the fluorescent lipid. The SUVs will bind to the coverslip surface, rupture, and then fuse with each other to form a flat bilayer.
5. After the incubation, the solution is then washed repeatedly with Vesicle Buffer to remove the excess vesicles which have not adhered to the surface. Then, the bilayer is immersed in approximately 0.5 mL of 1 × F-buffer that does not contain ATP.
6. At this point, the chamber is mounted on the microscope and FRAP is performed to assess the quality of the bilayer. A circular spot of approximately 10 μm in diameter is bleached for 5 s using a 491 nm Mosaic laser. The bilayer is then imaged (Oregon Green DHPE) every 2 s for approximately 30 s. The fluorescence recovers completely in approximately 10–15 s.
7. The quality of the bilayer is further assessed by the uniformity of the fluorescence and the lack of any large aggregates of lipid which may have

been leftover from the SUV deposition. Often, there are scratches on the surface of the coverslip to which no lipid will bind. During the experiment, we avoid imaging the contraction of the network near these regions, as actin and myosin will stick to the coverslip.

4.2. Construction and contraction of F-actin cortex

4.2.1 Introduction of F-actin

The F-actin is not polymerized within the sample chamber, but separately in a 0.5 mL microcentrifuge tube and then added to the bilayer. This is done as to not adhere incompletely polymerized F-actin to the bilayer, and thereby influence the kinetics of polymerization and equilibrium length of the filaments. The steps are as follows:

1. In a 500 μL microcentrifuge tube, 2.0 μ*M* dark actin and 0.6 μ*M* fluorescent actin (Alexa 568, Molecular Probes) are combined with 4 μ*M* dark phalloidin (Cytoskeleton) in 1 × F-buffer. The solution is supplemented with 0.5% methylcellulose (14,000 MW, Sigma), 9% glucose oxidase/catalase (Calbiochem), and glucose. This solution is incubated on ice for 1.5–2 h.
2. Afterwards, this 500 μL polymerization mix is then added to the 500 μL solution that immerses the bilayer, dividing the concentration of methylcellulose, F-actin, and ATP by 2, leaving 0.25% methylcellulose, 1.3 μ*M* actin, and 0.250 m*M* ATP. The F-actin is allowed to accumulate on the surface of the bilayer for 15 min (Fig 15.4A). Although minimal bundling is observed in this 2D assay, a 0.2% methylcellulose solution has been shown to initiate bundle formation in 3D assays (Kohler, Lieleg, & Bausch, 2008).

4.2.2 Attachment of F-actin to membrane

For the attachment of F-actin to the bilayer membrane, we utilize FimA2 (pET-21a-MBP-FimA1A2p-His, gift of Dave Kovar, University of Chicago), a mutant construct of the actin cross-linker Fimbrin containing a single F-actin-binding domain (Skau et al., 2011). FimA2 has a His-tag; therefore, it can simultaneously bind the nickel lipid in the membrane as well as a single F-actin. It is added following bilayer membrane formation and prior to F-actin addition. It is added at varying concentrations that correspond to different degrees of immobilization of F-actin. We choose three concentrations: 10, 100, and 1000 n*M* FimA2 for low, medium, and high levels of adhesion. Below 10 n*M* FimA2, F-actin is completely mobile on

the membrane surface as can be seen by the fluctuation of the F-actin. By the same metric, at 1 μ*M* FimA2, F-actin is completely immobile. Regardless of concentration, FimA2 is incubated on the membrane for 15 min.

1. Add volume of FimA2 to 0.5 mL of ATP-free F-buffer. Incubate on membrane for 15 min.
2. Wash repeatedly with ATP-free F-buffer. The stability of the nickel–His bond is strong, such that very little FimA2 leaves the surface of the membrane.

4.2.3 F-actin cross-linking

The presence of F-actin cross-linking proteins links individual F-actin, thereby increasing the length scale of contraction by myosin activity (Janson et al., 1991). In addition, cross-linking proteins can change the architecture of the network itself, from primarily filamentous to highly bundled. The type of cross-linker may also join filaments based on their polarity.

To cross-link our F-actin network, we include the cortical F-actin cross-linker α-actinin. α-Actinin is known to bind F-actin without bias on the orientation of the filaments. Furthermore, at low concentrations (1:300 [α-actinin]:[actin]) links F-actin isotropically, but can bundle F-actin at high concentrations (1:30 [α-actinin]:[actin]). Thus, the architecture as well as the connectivity of the network is modified by α-actinin.

1. After the sedimentation of the F-actin, add the desired volume of α-actinin to 100 μL F-buffer, and add this volume to the center of the chamber. The protein will diffuse throughout the chamber and bind the F-actin network.
2. Regardless of the concentration, incubate the α-actinin in the chamber for 15 min (Fig 15.4B). If 1:30 [α-actinin]:[actin] concentration, bundling can be observed to assess the completion and spatial uniformity of cross-linking.

4.2.4 Myosin II addition

After cross-linking, varying concentrations (10–100 n*M*) of skeletal muscle myosin II dimers are added to the sample chamber. The myosin dimers are small and diffuse quickly through the chamber. They polymerize into thick filament assemblies within minutes, bind the F-actin network, and induce contraction (Fig 15.4C). For highly cross-linked samples (1:300 [α-actinin]:[actin]), the F-actin network is highly connected. When myosin is added, the entire network contracts with a length scale larger than the

microscope field of view and may be centered anywhere across the 25-mm coverslip (Fig. 15.5).

To spatially control the contraction, we have successfully used the property that the myosin II ATPase inhibitor, blebbistatin, is inactivated by short exposure (100 ms) to low power (>0.1 mW/μm^2) light with wavelength <500 nm (Sakamoto, Limouze, Combs, Straight, & Sellers, 2005). When using this approach, 40 μM blebbistatin is added after the formation of a lipid bilayer. Thus, when the F-actin is crowded to the surface of the bilayer, the solution is well mixed. After the myosin is added, it polymerizes, accumulates on the F-actin surface, and is weakly bound to F-actin, but its mechanochemical activity is inhibited. This method is therefore suitable for highly cross-linked networks, as the presence of blebbistatin-inhibited myosin itself introduces a small degree of cross-linking but is minor compared to the binding of passive cross-linkers at high concentrations such as α-actinin. Then, upon illumination of the network with the 491 nm light, the myosin inhibition is released, and the network contracts, centered within out field of view.

4.2.5 Sources of variability

Local organization of F-actin: F-actin that is crowded to the surface of the bilayer membrane in the absence of adhesion orders itself quasi-nematically (Fig. 15.4). Thus, there are local regions of F-actin alignment, which may vary across a $60\times$ field of view. As we expect that network architecture may modulate contractility, the contraction of the network will vary across the field of view as well. Adhesion of the F-actin to the membrane abrogates this variability. As the nematic alignment of F-actin is thermal, very low adhesion would be required to eliminate this effect.

Size of myosin thick filaments: The myosin is added as dimers in solution after the sedimentation of F-actin. During incubation within the chamber, the myosin polymerizes into thick filaments, as it transitions from its 0.45 M KCl buffer into a 50 mM KCl buffer. However, the size of the thick filaments will vary with the dimer concentration added. Thus, in the future, myosin thick filaments should be preformed and introduced into the chamber fully polymerized.

5. FUTURE DIRECTIONS

Over the past several years, we have successfully used these assays to identify the requirements and regulation of actomyosin contractility in both bundles and networks. By systematically changing the myosin density, we

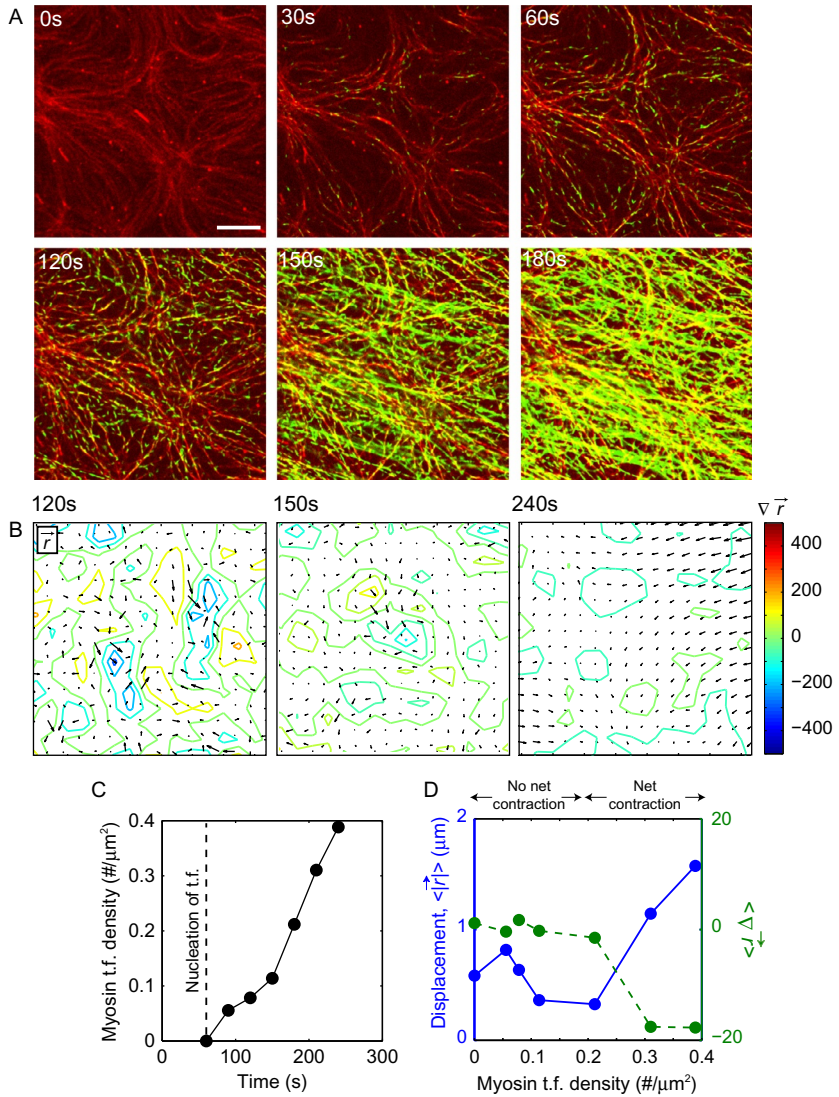

Figure 15.5 Quantification of F-actin network contractility. (A) F-actin (red) and smooth muscle myosin II (green) within a contracting model cortex. Myosin accumulates over time. Scale bar is 10 μm. (B) Overlay of F-actin displacement (*r*, black arrows) and divergence of F-actin displacement (colored contours) for the contracting network in (A). Hot colors indicate positive divergence (expansion) and cool colors indicate negative divergence (contraction). (C) Myosin thick filament density ρ, over time. (D) Mean divergence (green) and speed (blue) of the F-actin displacement (*r*) as a function of myosin thick filament density, *r*.

have identified a critical myosin density necessary for contraction (Thoresen et al., 2011) and determined how the myosin filament properties (size and isoform composition) regulate the contraction rate (Thoresen et al., 2013). We have also explored how myosin-driven stresses can result in self-organization of a sarcomere-like structure within bundles (Stachowiak et al., 2012). Finally, we have demonstrated the importance of F-actin bending and buckling in facilitating contraction in disordered actomyosin arrays (Lenz, Gardel, & Dinner, 2012; Lenz, Thoresen, Gardel, & Dinner, 2012; Murrell & Gardel, 2012). The semi-flexibility of F-actin is crucial to break the symmetry between tensile and compressive stresses generated in disordered actomyosin bundles (Lenz, Gardel, & Dinner, 2012) and networks to facilitate robust contractility over a wide range of network architectures (Lenz, Gardel, & Dinner, 2012; Lenz, Thoresen, Gardel, & Dinner, 2012; Murrell & Gardel, 2012). Moreover, we have found that myosin II-generated filament bending results in F-actin severing, thus providing a putative mechanism for coordinating contraction and actin filament polymerization dynamics in contractile systems.

We can now explore the phase space of these motor-filament bundles and networks to determine the regulation of contractility by changing parameters involving the filaments (bending rigidity, length, density), motors (myosin II isoform and thick filament size), and accessory proteins (F-actin assembly factors and cross-linkers, cross-linkers between the membrane and F-actin network). We anticipate such experiments will identify how contractility is spatially regulated in the cellular cortex to support diverse morphological processes. Through addition of F-actin assembly factors, we can attempt to reconstitute the steady-state dynamic contractile arrays observed to understand the coordination of F-actin assembly, contraction and disassembly observed in diverse systems such as the lamella and cytokinetic ring. Moreover, we anticipate these experiments will shed light on how strains and forces within contractile arrays are used to drive changes in the association of regulatory factors such as α-actinin (Aratyn-Schaus, Oakes, & Gardel, 2011) and zyxin (Smith et al., 2010). Finally, this assay can be utilized to explore the interplay between myosin-driven actin dynamics and membrane organization, a crucial interface that determines cellular response to chemical and physical stimuli from the external environment (Kapus & Janmey, 2013). Eventually, as these processes are revealed, these studies will facilitate the reconstitution of artificial cells by compartmentalization of crucial factors inside vesicles (Carvalho et al., 2013).

ACKNOWLEDGMENT

M. G. is funded by a Burroughs Wellcome Career Award at the Scientific Interface and the Packard Foundation. We thank Patrick McCall for a careful reading of the chapter.

REFERENCES

Aratyn-Schaus, Y., Oakes, P. W., & Gardel, M. L. (2011). Dynamic and structural signatures of lamellar actomyosin force generation. *Molecular Biology of the Cell*, *22*, 1330–1339.

Aratyn-Schaus, Y., Oakes, P. W., Stricker, J., Winter, S. P., & Gardel, M. L. (2010). Preparation of compliant matrices for quantifying cellular contraction. *Journal of Visualized Experiments,* (46).

Bárány, M. (1996). *Biochemistry of smooth muscle contraction*. San Diego: Academic Press.

Carvalho, K., Tsai, F. C., Lees, E., Voituriez, R., Koenderink, G. H., & Sykes, C. (2013). Cell-sized liposomes reveal how actomyosin cortical tension drives shape change. *Proceedings of the National Academy of Sciences of the United States of America*, *110*(41), 16456–16461.

Dainty, M., Kleinzeller, A., Lawrence, A. S., Miall, M., Needham, J., Needham, D. M., et al. (1944). Studies on the anomalous viscosity and flow-birefringence of protein solutions: III Changes in these properties of myosin solutions in relation to adenosine triphosphate and muscular contraction. *Journal of General Physiology*, *27*(4), 355–399.

Ebashi, S., & Ebashi, F. (1964). A new protein factor promoting contraction of actomyosin. *Nature*, *203*, 645–646.

Huxley, H. E. (2004). Fifty years of muscle and the sliding filament hypothesis. *European Journal of Biochemistry*, *271*(8), 1403–1415.

Janson, L. W., Kolega, J., & Taylor, D. L. (1991). Modulation of contraction by gelation/solation in a reconstituted motile model. *Journal of Cell Biology*, *114*(5), 1005–1015.

Kapus, A., & Janmey, P. (2013). Plasma membrane—Cortical cytoskeleton interactions: A cell biology approach with biophysical considerations. *Comprehensive Physiology*, *3*, 1231–1281.

Kohler, S., Lieleg, O., & Bausch, A. R. (2008). Rheological characterization of the bundling transition in F-actin solutions induced by methylcellulose. *PLoS One*, *3*(7), e2736.

Lenz, M., Gardel, M. L., & Dinner, A. R. (2012). Requirements for contractility in disordered cytoskeletal bundles. *New Journal of Physics*, *14*(3), 033037.

Lenz, M., Thoresen, T., Gardel, M. L., & Dinner, A. R. (2012). Contractile units in disordered actomyosin bundles arise from F-actin buckling. *Physical Review Letters*, *108*(23), 238107.

Margossian, S. S., & Lowey, S. (1982). Preparation of myosin and its subfragments from rabbit skeletal muscle. *Methods in Enzymology*, *85*(Pt. B), 55–71.

Murrell, M. P., & Gardel, M. L. (2012). F-actin buckling coordinates contractility and severing in a biomimetic actomyosin cortex. *Proceedings of the National Academy of Sciences of the United States of America*, *109*(51), 20820–20825.

Pollard, T. D. (1982). Myosin purification and characterization. *Methods in Cell Biology*, *24*, 333–371.

Sakamoto, T., Limouze, J., Combs, C. A., Straight, A. F., & Sellers, J. R. (2005). Blebbistatin, a Myosin II inhibitor, is photoinactivated by blue light. *Biochemistry*, *44*(2), 584–588.

Skau, C. T., Courson, D. S., Bestul, A. J., Winkelman, J. D., Rock, R. S., Sirotkin, V., et al. (2011). Actin filament bundling by fimbrin is important for endocytosis, cytokinesis, and polarization in fission yeast. *Journal of Biological Chemistry*, *286*(30), 26964–26977.

Smith, M. A., Blankman, E., Gardel, M. L., Luettjohann, L., Waterman, C. M., & Beckerle, M. C. (2010). A zyxin-mediated mechanism for actin stress fiber maintenance and repair. *Developmental Cell*, *19*(3), 365–376.

Spicer, S. S. (1951). Gel formation caused by adenosine triphosphate in actomyosin solutions. *Journal of Biological Chemistry*, *190*(1), 257–267.

Stachowiak, Matthew R., McCall, Patrick M., Thoresen, T., Balcioglu, Hayri E., Kasiewicz, L., Gardel, Margaret L., et al. (2012). Self-organization of Myosin II in reconstituted actomyosin bundles. *Biophysical Journal*, *103*(6), 1265–1274.

Stossel, T. P., Hartwig, J. H., Yin, H. L., Zaner, K. S., & Stendahl, O. I. (1982). Actin gelation and structure of cortical cytoplasm. *Cold Spring Harbor Symposia on Quantitative Biology*, *46*(Pt. 2), 569–578.

Szent-Györgyi, A. (1945). Studies on muscle. *Acta Physiologica Scandinavica*, *9*, 1–116.

Szent-Györgyi, A. (1947). *Chemistry of muscular contraction*. New York: Academic Press.

Szent-Gyorgyi, A. (1950). Actomyosin and muscular contraction. *Biochimica et Biophysica Acta*, *4*(1–3), 38–41.

Thoresen, T., Lenz, M., & Gardel, M. L. (2011). Reconstitution of contractile actomyosin bundles. *Biophysical Journal*, *100*(11), 2698–2705.

Thoresen, T., Lenz, M., & Gardel, M. L. (2013). Thick filament length and isoform composition determine self-organized contractile units in actomyosin bundles. *Biophysical Journal*, *104*(3), 655–665.

Watanabe, S., & Yasui, T. (1965). Effects of magnesium and calcium on the super precipitation of Myosin B. *Journal of Biological Chemistry*, *240*, 105–111.

Weber, A., & Winicur, S. (1961). The role of calcium in the superprecipitation of actomyosin. *Journal of Biological Chemistry*, *236*, 3198–3202.